Atmospheric Research 299 (2024) 107167

Contents lists available at ScienceDirect

Atmospheric Research

journal homepage: www.elsevier.com/locate/atmosres

Climatology and trends of cirrus geometrical and optical properties in the Amazon region from 7-yr of CALIPSO observations

Ben-hur Martins Portella [a], Henrique de Melo Jorge Barbosa [b,*]

[a] Physics Institute, University of São Paulo, Rua do Matão, 1371, São Paulo 05508-900, São Paulo, Brazil
[b] Physics Department, University of Maryland Baltimore County, 1000 Hilltop Cir., Baltimore 21250, MD, United States

ARTICLE INFO

Keywords:
Amazon rainforest
Cirrus clouds
CALIOP
Spatial distribution
Trends

ABSTRACT

Recent studies have shown that the presence of cirrus clouds in the Amazon is higher than in other tropical regions, but also that convective activity in the region is decreasing, which could mean a decrease in high clouds. We used data from 2009 to 2016 from Cloud-Aerosol Lidar with Orthogonal Polarization (CALIOP), aboard Cloud-Aerosol Lidar and Infrared Pathfinder Satellite Observations (CALIPSO), to study cirrus over the Amazon. Here we report on an analysis of the frequency of occurrence, base and top altitude, geometric thickness, and optical depth for the whole Amazon, as well as their spatial distribution and medium-term trends. A total of 1,473,863 vertical profiles were analyzed containing 728,123 cirrus layers, being 37.0% in the wet and 21.2% in the dry season. They are evenly distributed throughout the region during the wet season and concentrated in the northwest of the Amazon during the dry season. In terms of cloud optical depth (COD), most cirrus were optically thin ($0.03<COD<0.3$), with a relative frequency of 43.9%, while subvisual ($COD<0.03$) and thick ($COD>0.3$) corresponded to 22.0 and 34.1%, respectively. The results indicate a significant reduction in the frequency of cirrus occurrence of $1.3 \pm 0.3\%$ per year in the wet season, accompanied by a reduction of the geometric thickness of the thickest cirrus by 57 ± 18 m. This corroborates previous reports of a reduction of convective activity and high cloud fraction in the region.

1. Introduction

Clouds cover about 70% of the planet's surface (Lohmann et al., 2016) and are key elements of the climate system. They can participate in both the terrestrial albedo and the re-emission of thermal radiation, depending on their macro and microphysical properties (Liou, 2002; Trenberth, 2022). However, they manifest enormous spatial and temporal variability, which makes their representation in computational models difficult. In fact, the greatest uncertainties in forecasts for the future climate are related to uncertainties in the distribution and properties of clouds and aerosols, as well as the interactions between them (Solomon et al., 2007), a reality that has persisted in recent decades (Stocker et al., 2013; Arias et al., 2021).

Among the different types of clouds are cirrus, which are high clouds made entirely of ice crystals, with a cloud base above 8 km, and a cloud top temperature below −37° (e.g., Seifert et al., 2007; Campbell et al., 2015). In the tropics, these clouds are commonly formed from deep convection through the detachment and dispersion of the anvils (Liou, 2002; Larsgård, 2008; Gouveia, 2018). They remain for hours or days in the atmosphere and have a net warming effect (Liou, 2002; Lee et al., 2009; Berry et al., 2019). Given the high incidence of solar radiation and the warm temperatures, tropical cirrus have an important radiative effect in both the short and long wavelengths (Gouveia, 2018). Hence, changes in their properties could aggravate or ameliorate global warming (Zhu, 2011). Hence, understanding cirrus properties and how they might be changing, particularly in the tropics is of utmost importance.

Over the Amazon, Gouveia et al. (2017) performed the characterization of optical and geometric properties of cirrus near the city of Manaus, using one year of data from a ground-based lidar system. They found higher frequencies of occurrence than those reported for other tropical regions, with values above 50% in the dry season and reaching up to 88% during the wet season. Sena et al. (2018) used data from *International Satellite Cloud Climatology Project* (D1 product) and *Geostationary Operational Environmental Satellites* (GOES)-6,-7,-8 and −12, to investigate the variability in the seasonal cycle of convection in the Amazon basin. They noted a significant reduction in cloud cover over the past few decades, with a maximum rate of reduction of about 6% per

* Corresponding author.
E-mail address: hbarbosa@umbc.edu (H.M.J. Barbosa).

https://doi.org/10.1016/j.atmosres.2023.107167
Received 28 June 2023; Received in revised form 5 December 2023; Accepted 5 December 2023
Available online 14 December 2023
0169-8095/Published by Elsevier B.V.

year at 1200 UTC (0800 LT) in central and eastern Amazon. They also found that the drop in the high cloud cover fraction is the main factor contributing to this reduction in the overall cloud cover in this region.

The present study aimed to characterize cirrus clouds over the Amazon and assess whether there are significant trends in their properties. We used data from the *Cloud-Aerosol Lidar with Orthogonal Polarization* (CALIOP), aboard the *Cloud-Aerosol Lidar and Infrared Pathfinder Satellite Observations* (CALIPSO) for the entire Amazon and the period 2006–2019, as described in Section 2. We present a cirrus climatology including frequency of occurrence and optical and geometric properties for the entire region and period studied. We then evaluate their spatial distribution and estimate possible future trends in these properties (Section 3), finally leading to the discussions and conclusions set out in Section 4.

2. Materials and methods

2.1. CALIOP observations

Launched in 2006, CALIPSO has provided a detailed description of the atmosphere (Winker et al., 2010). CALIOP, its main instrument, is a dual-wavelength lidar acquiring vertical elastic backscatter profiles at 532 and 1064 nm. The observation angle is close to nadir, about 0.3° from launch until November 2007 and 3.0° thereafter. It also measures the volume depolarization ratio at 532 nm that, combined with the attenuated backscatter coefficients, is used for the discrimination between water and ice phases in clouds, as well as to identify non-spherical aerosol particles (Hu et al., 2009; Avery et al., 2020). Its sampling resolution (both horizontal and vertical) varies with altitude, with samples being averaged according to the height in which they are identified (Vaughan et al., 2009, 2023).

The latest major release of CALIPSO data set is version 4.00 from April 2014, which was later updated to 4.10 in November 2016, and 4.20 in October 2018 NASA (2022). Improvements in the calibration for the V4 relative to the V3 datasets are described by Getzewich et al. (2018) and Kar et al. (2018). In the present work, cloud layer data products (hereafter "CLay" product), level 2, version 4.20, with horizontal resolution of 5 km are used (NASA/LARC/SD/ASDC, 2018). This product includes layers detected at 5, 20, and 80 km horizontal resolution, which corresponds to averaging over 15, 60, and 240 single profiles, respectively. We select the CALIPSO satellite tracks within coordinates 12.5°S - 2.5°N and 50°W - 74°W, from June 2006 to December 2019. Fig. 1 shows the set of tracks covering the selected area, which we take as representative of the Amazon biome (indicated in green).

Occasional failures in the operation of the CALIOP can affect measurements globally, reducing data availability in the study region. From 2006 to 2019, the number of Clay profiles available every month was 17,671 ± 2909, or about 89% of the average expected amount of 19,846. The large standard deviation means that some months have as little as 50% of the expected data, which will have to be considered in our statistical analysis.

Another important factor is the reduction in the pulse energy due to a problem with the laser in CALIOP, which affected data in 2008 and after September 2016. Lower laser pulse energy means a reduced signal-to-noise ratio, which compromises signal quality. This effect occurs most frequently in the *South Atlantic Magnetic Anomaly* (SAA) region, which extends mainly over the southeast of South America but also reaches into the Amazon domain (see Fig. 16 by Hunt et al., 2009). The greater flux of cosmic radiation over the SAA also affects the photomultipliers, enhancing the measurement noise and posing challenges to the calibration and retrievals (Noel et al., 2014). However, these were minimized in CALIOP's algorithm version 4, which uses an adaptive spike filter to remove outliers and reduce the difference in the nighttime calibration coefficients over the SAA and non-SAA regions (see details in Kar et al., 2018). Moreover, a multi-orbit averaging scheme is now used to suppress the influence of the elevated noise-levels on the daytime data processing (Getzewich et al., 2018). Here, we follow the recommendation from the CALIPSO technical advisory team and discard those profiles with minimum laser energy at 532 nm less than 80 mJ (NASA, 2018). Hereafter, these are called "bad" profiles, while those with minimum laser energy equal or above 80 mJ are "good" profiles.

Fig. 2a shows the percentage of "bad" profiles within our study region, separated between day and night. The plot shows a significant increase from the second half of 2016 onward. A similar problem had already occurred around 2007 and 2008, which was resolved by switching the spare laser on. Fig. 2b shows the spatial distribution of the fraction of profiles affected by the reduction in laser energy, averaged over the affected years only. There is a higher concentration of unusable data in the southeastern part of the Amazon, which imposes further challenges to the analysis.

Therefore, we consider the 7-year period between Jun-2009 and

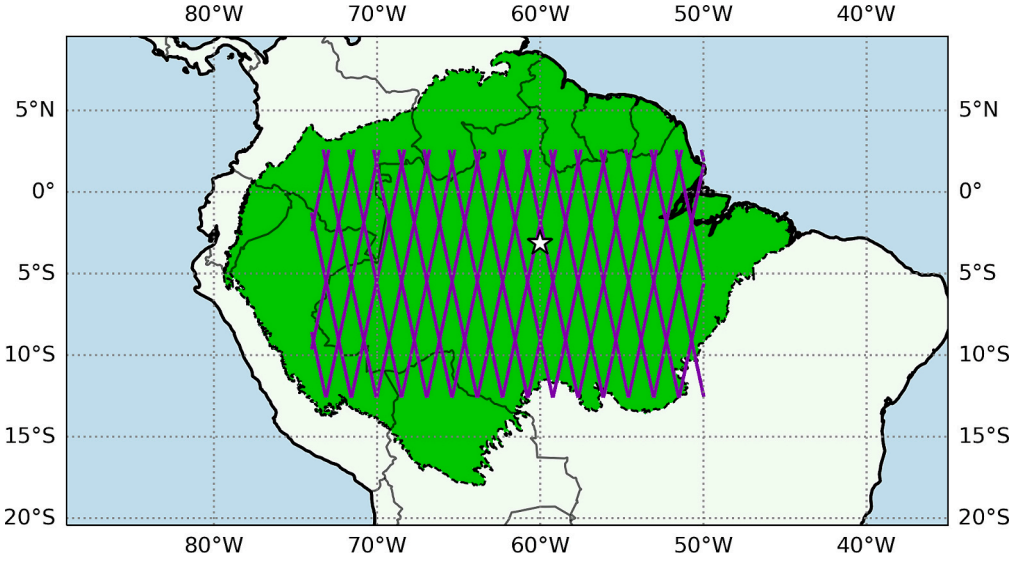

Fig. 1. Area covered by the tracks (in violet) of CALIPSO in the chosen region. The area in green represents the Amazon biome, and the star indicates the location of the ground-based lidar used by Gouveia et al. (2017), near the city of Manaus. (For interpretation of the references to colour in this figure legend, the reader is referred to the web version of this article.)

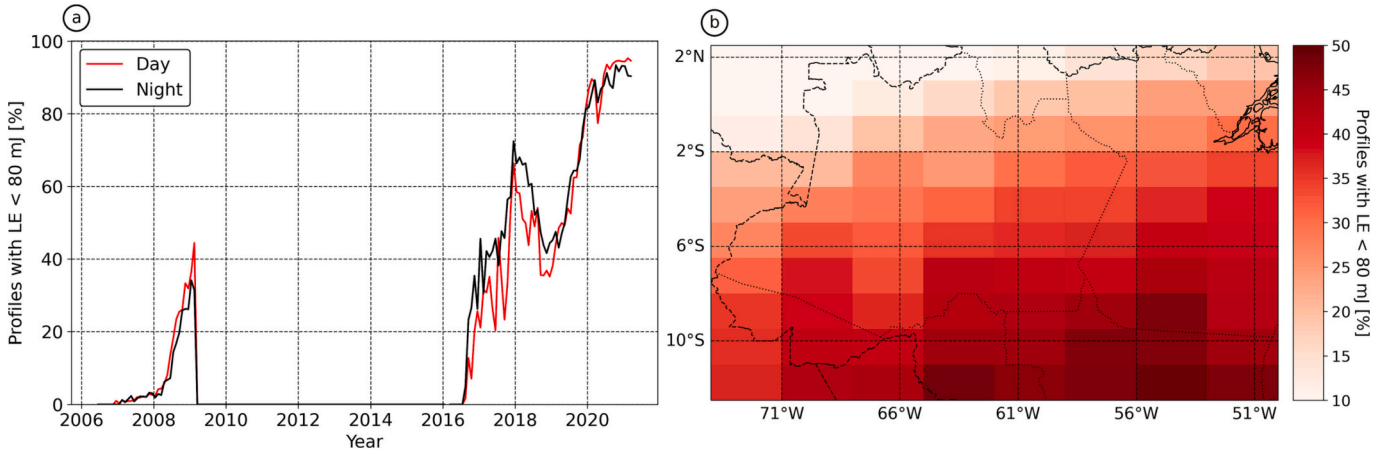

Fig. 2. (a) Percentage of profiles in the Amazon region with 532 nm laser energy below 80 mJ, divided into day and night. (b) Mean percentage of profiles with laser energy below 80 mJ calculated over months with a non-negligible percentage of profiles considered "bad" (from 11–2006 to 02–2009 and from 07–2016 to 12–2019).

May-2016 for our scientific analysis. Our aim is to describe the general properties of the cirrus clouds in the Amazon rainforest, hence we focus on the longest continuous period without low energy profiles, so that data coverage is uniform spatially and temporally.

2.2. Identification of cirrus layers

The CLay product reports on atmospheric layers classified by the Scene Classification Algorithm (SCA). The SCA discriminates between aerosol and clouds using the layer-mean attenuated backscatter at 532 nm and the attenuated colour ratio (Liu et al., 2005). For the cloud layers, the SCA distinguishes between the different cloud phases based on the layer-mean volume depolarization ratio and the layer-integrated attenuated backscatter at 532 nm (Hu et al., 2009; Avery et al., 2020). The cloud sub-typing uses the cloud top pressure, cloud fraction, and transparency. According to Liu et al. (2005), cirrus are transparent clouds with top pressure below 440 mb. Opaque cirrus are included in a broad category that includes cumulus nimbus, altostratus, and nimbostratus, all opaque clouds with high tops that are indistinguishable from CALIOP's perspective because of the apparent bottom altitude.

For our analysis, we consider cirrus to be cloud layers (feature type = 2), classified as cirrus-transparent (sub-type = 6), and composed of ice or oriented ice (phase = 1 or 3). We further require they have a base altitude above 8 km and a top temperature below −37 °C, following similar thresholds used in previous studies (e.g., Seifert et al., 2007; Campbell et al., 2015; Gouveia et al., 2017), which helps selecting cloud layers composed of ice crystals only. Moreover, to ensure the quality of the classification and the optical retrievals, we combine different quality flags. We restrict the analysis to layers with a high confidence in their feature classification (Feature QA = 3), which corresponds to a Cloud-Aerosol Discrimination score above 70%, and a high confidence in the phase classification (Phase QA = 3). In addition, we used the Extinction Quality Check to guarantee the quality of the optical retrieval for the individual layers, i.e., of the retrieved extinction and backscattering coefficients. We follow the CALIPSO Quality Summary recommendation and selected layers with an Extinction QC flag of either 0 or 1 (NASA, 2023).

2.3. Pre-processing profiles and cirrus layers

We process the CLay data files twice. The first pre-processing routine generates a table of profiles. Each table entry has the basic information from each CLay profile as well as derived information to help our analysis. The basic information includes: Year, month, and day of detection; Day or night orbit; Latitude and longitude; Tropopause height; and laser pulse energy. We calculate: Month numbering (since June-2006); Profile number (from the first measured); Position (i,j) in a regular grid; and Presence or not of cirrus layers according to our criteria. Creating a regular grid allows to group the along-track data in bins of latitude and longitude for spatial analysis. The position and spacing of the cells, 1.5° latitude by 3° longitude, are chosen so that the number of profiles in each cell is approximately the same.

The second pre-processing routine generates a table of cirrus layers. For each cirrus layer, we save the basic and derived information from the CLay profile (same as above), together with the information from the cirrus layer: Base and top altitude; Base and top temperature; and Optical depth and its uncertainty. In addition, we check for vertical overlap when multiple layers are reported in the same profile. The CLay product relies on a nested multi-grid feature finding algorithm that searches for layer boundaries at multiple averaging resolutions (Vaughan et al., 2005). As a result, different parts of the same cloud layer might be reported as independent layers detected at different resolutions (5, 20, or 80 km), which might overlap or be very close together. Here we follow Thorsen et al. (2013) and merge the boundaries of neighbouring layers that are closer than 1 km. The merged layer's top altitude and temperature are taken from the layer on top, while bottom altitude and temperature are taken from the layer beneath. The CODs are added, and the CODs uncertainties are propagated.

2.4. Statistical analysis

The analysis is performed separately for the different seasons: wet (January to April), dry (June to September), and transition (May and October to December). The analysis is also segregated in terms of the cloud optical depth (COD), and results are presented for subvisual (SVC) (COD < 0.03), thin (0.03 < COD < 0.3), and thick (COD > 0.3) layers. These are the same thresholds proposed by Sassen and Cho (1992), with a caveat: we use the term "thick" in distinction from "opaque". As explained in the previous session, our analysis considers transparent layers only; hence we avoid the "opaque" terminology as these thick layers do not fully attenuate the CALIOP's signal.

The general statistical characterization of cirrus clouds, i.e. the cirrus climatology, includes the mean and standard deviation of cloud base and top altitudes, cloud geometric thickness, and cloud optical depth, as well as the frequency of occurrence. The frequency of occurrence refers to the fraction of the observation period in which cirrus clouds are observed over the Amazon. For a particular time (month, season, or year) and location (a cell or the whole region), this is the ratio of the number of profiles with at least one cirrus layer divided by the number of "good" profiles, i.e.,

$$f(time, loc) = \frac{N_{cirrus}(time, loc)}{N_{total}(time, loc)} \quad (1)$$

The analysis of the spatial distribution of the optical and geometric properties is carried out with maps where each cell shows the median (or a different percentile) of the corresponding property in a given season. In each cell, the statistic is calculated from all the data for a particular time (month, season, or year).

2.5. Trends and uncertainties

To analyze the possible trends in the cirrus optical and geometrical properties, we perform a linear regression on the annual percentiles time series considering their uncertainty, thereby obtaining the slope and the associated error. The statistical significance of the slope, i.e., whether there is a trend or not, is verified with a Student's *t*-test (Wilks, 2006) considering a significance level of 95%. The uncertainties associated with the percentiles are estimated using the bootstrap technique (Efron, 1982). Data for a given year is randomly resampled $N = 100$ times, allowing for repetition. The percentile is calculated for each new sample, yielding a set of *N* percentiles. Finally, the uncertainty in the percentile is estimated by the standard deviation of this set. The process is repeated for data from subsequent years. This same technique is applied to determine the uncertainties of the frequency of occurrence. The trends are calculated for the domain-averaged time series or for the time series in individual cells, in which case the spatial distribution of the trends can be analyzed.

3. Results and discussion

3.1. Climatology: wet × dry seasons

To build the climatology, 1.4 million CLay profiles with 5 km resolution were analyzed from 1-Jun-2009 to 31-May-2016, and cirrus clouds were observed in about 49.4% of these. Table 1 summarizes the vertical profile statistics. There is a marked seasonal cycle in the frequency of occurrence, with a minimum of 24.6% in August, and a maximum of 66.5% in December. In terms of seasons, the frequency of occurrence is minimum during the dry (June to September, mean 31.1%) and maximum during the wet season (January to April, mean 59.2%). The seasonality in total cirrus optical depth is much lower. Varying from 0.44 in the wet to 0.38 in the dry season, or about 16%. Similarly, the number of cirrus layers in each cloudy profile varies only between 1.14 in the wet (16.7% cloudy profiles are multi-layer) to 1.08 in the dry (9.6% are multi-layer) season, or about 5%.

Considering all profiles analyzed, a total of 819,805 layers of cirrus clouds were detected over the Amazon. Table 2 presents the statistics for all registered layers. The mean base altitude of cirrus clouds is 13.2 ± 2.1 km, while the mean top is 15.4 ± 1.8 km, resulting in a mean geometric thickness of 2.16 ± 1.47 km. Both the base and the top are higher in the wet season than in the dry season, by about 6%, because of the change in the tropopause altitude. The geometric thickness, however, shows a larger variation throughout the year, varying from 1.9 km (dry) to 2.22 km (wet). Another notable difference between the wet and dry seasons is the fraction of cirrus tops above the tropopause (30.8 and 20.0%, respectively). The mean optical depth is 0.38 ± 0.57, and the relative frequency of thin cirrus (43.9%) is much higher than thick (34.1%) and subvisual cirrus (22.0%) on average, with little seasonal changes.

Over the Amazon, the observed seasonality in the frequency of occurrence and other cirrus properties are linked mainly to the changes in precipitation rates throughout the year, but also to changes in circulation and temperature near the top of the troposphere (Gouveia et al., 2017). Fig. 3a and b show the precipitation in the wet and dry seasons from 2009 to 2016. They help explain the spatial distributions of cirrus, which are shown in Fig. 3c and d. During the wet season, there is a relatively uniform distribution of clouds, with a frequency around 60% and a slight concentration in the southeastern region. This uniformity follows the expanse of areas intensely covered by precipitation during the wet season, as seen in Fig. 3a.

In the dry season, the frequency of occurrence decreases significantly, falling to values of 30% or less in the southeastern portion. There is a greater concentration of clouds in the northwest of the Amazon, close to Colombia and Venezuela, where the highest precipitation rates

Table 1
Summary of integrated statistics on cirrus profiles for wet, dry, transition seasons and full year, from 2009 to 2016. Standard deviations are shown in parentheses.

	Total	Wet	Transition	Dry
No. of profiles	1,473,863	455,898	520,636	497,329
No. of profs. w/ cirrus	728,123	270,022	303,653	154,448
Frequency of occurrence (%)	49.4	59.2	58.3	31.1
Total cirrus optical depth[1,2]	0.42 (0.6)	0.44 (0.61)	0.43 (0.61)	0.38 (0.58)
Number of cirrus layers[2]	1.13	1.14	1.14	1.08
Profs. w/ 1 cirrus layer (%)	85.1	83.3	84.2	90.4
Profs. w/ 2 cirrus layers (%)	14.2	16.0	15.1	9.4
Profs. w/ 3 cirrus layers (%)	0.6	0.7	0.7	0.2

[1] Sum of the COD from the cirrus layers in the same profile.
[2] Average over profiles with cirrus.

Table 2
Summary statistics on cirrus layers for the wet (Jan-Apr), dry (Jun-Sep), transition (May, Oct-Dec) seasons and full year, over the period 2009 to 2016. Standard deviations are shown in parentheses. Occurrence of thick, thin, and SVC cirrus is given as relative frequencies.

	Total	Wet	Transition	Dry
All layers				
No. of cirrus layers	819,805	308,524	344,783	166,498
Base altitude (km)	13.2 (2.1)	13.4 (2.2)	13.3 (2.1)	12.7 (1.9)
Top altitude (km)	15.4 (1.8)	15.6 (1.8)	15.5 (1.8)	14.6 (1.6)
Geometric Thickness (km)	2.16 (1.47)	2.22 (1.52)	2.25 (1.5)	1.9 (1.25)
Layer optical depth	0.38 (0.57)	0.38 (0.58)	0.38 (0.58)	0.35 (0.56)
Thick cirrus (%)	34.1	34.9	34.8	31.3
Thin cirrus (%)	43.9	42.8	44.1	45.8
SVC (%)	22.0	22.4	21.1	23.0
Base > tropop. (%)	1.5	1.7	1.7	0.8
Top > tropop. (%)	29.0	30.8	31.8	20.0
Thick layers				
No. of cirrus layers	279,509	107,569	119,888	52,052
Base altitude (km)	11.6 (1.7)	11.7 (1.7)	11.6 (1.7)	11.1 (1.5)
Top altitude (km)	14.8 (1.9)	15.0 (1.9)	15.0 (1.9)	14.0 (1.6)
Geometric Thickness (km)	3.24 (1.64)	3.31 (1.69)	3.34 (1.65)	2.86 (1.43)
Thin layers				
No. of cirrus layers	360,285	131,960	152,147	76,178
Base altitude (km)	13.6 (1.7)	13.8 (1.7)	13.7 (1.6)	13.0 (1.5)
Top altitude (km)	15.4 (1.7)	15.7 (1.8)	15.6 (1.7)	14.7 (1.6)
Geometric Thickness (km)	1.88 (1.04)	1.92 (1.07)	1.94 (1.06)	1.69 (0.9)
SVC layers				
No. of cirrus layers	180,011	68,995	72,748	38,268
Base altitude (km)	15.0 (1.5)	15.3 (1.5)	15.1 (1.4)	14.2 (1.3)
Top altitude (km)	16.0 (1.5)	16.4 (1.5)	16.2 (1.4)	15.3 (1.4)
Geometric Thickness (km)	1.07 (0.56)	1.08 (0.58)	1.08 (0.58)	1.03 (0.5)

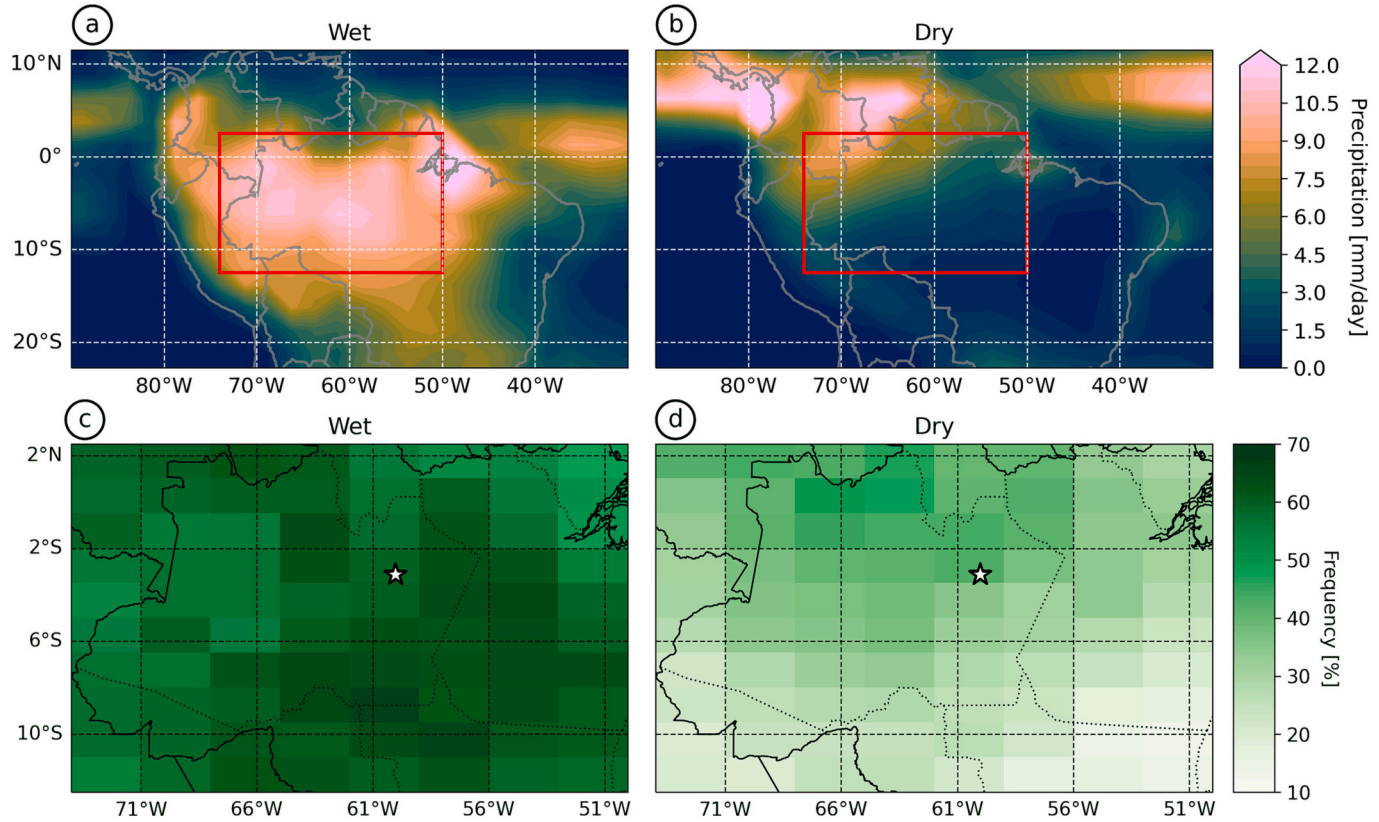

Fig. 3. Top: Maps of the average for precipitation (in mm/day) over the Amazon region, during (a) the wet season and (b) the dry season. The red rectangle corresponds to the analysis area. Data from the Global Precipitation Climatology Project (Adler et al., 2003). Bottom: Maps of cirrus frequency of occurrence during the wet season (c) and dry season (d). The star indicates the location of Manaus. Averages were calculated between Jun-2009 and May-2016. (For interpretation of the references to colour in this figure legend, the reader is referred to the web version of this article.)

are found. Over tropical forests, higher precipitation rates follow intense convective activity (Machado et al., 2002), which in turn means more detrainment of ice in the anvils and greater formation of cirrus clouds (Gouveia et al., 2017). This was first shown by Sassen et al. (2009), with maps of the global distribution of both deep convection (from CloudSat) and cirrus clouds (from CALIPSO). For the months of June to August, the authors found a greater presence of both types of cloud over Colombia and Venezuela.

Next, we look at the spatial patterns of the seasonal differences in the cirrus properties. Fig. 4 shows maps of base and top altitudes, geometric thickness, and optical depth, separated into wet and dry seasons. The right column shows the normalized histograms of these properties for the entire region. In the base and top altitude maps (panels a,b,d,e), it is noted that the values are spatially uniform during the wet season, while in the dry season, the altitudes are lower in the southeastern portion. During the wet season, the tropopause is higher, thus allowing the cirrus to reach higher altitudes, which is shown clearly by the histograms (panels c,f). Moreover, there is a larger population of clouds with tops above the tropopause during the wet season. The peaks observed in the base and top altitude distributions appear to occur in cirrus in general over the tropics, as reported by Nazaryan et al. (2008).

The geometric thickness maps show similar behavior. The wet season is spatially uniform, while a gradient pattern is found during the dry season, with thicker clouds toward Colombia and Venezuela and thinner clouds in the southeast. That is, geometric thicker cirrus layers close to the convective centers and thinner ones far away. We noticed, however, a sharp drop in the count of layers with geometric thicknesses below 500 m (Fig. 4i), which has not been observed by ground-based lidars. The distribution of geometric thicknesses presented by Gouveia et al. (2017), for instance, is similar to ours except for the smaller size bin (geometric thickness $<$ 500 m). The striking different remains even if we restrict the comparison to the satellite overpass times in the same 1-year period and location analyzed by Gouveia and coauthors (analysis not shown). This result indicates that CALIOP's algorithm has difficulty detecting such thin layers, likely due to a combination of small backscatter coefficients inside the cloud and low signal-to-noise ratio around the cloud (Gouveia, 2018). In principle, using newly developed algorithms could improve the detection of these thin layers (Vaillant De Guélis et al., 2021; Gouveia et al., 2017).

Regarding the COD, the maps in Figs. 4j,k show a similar picture. A visual inspection of the maps j-k and g-h shows higher COD values where higher geometric thickness is found. The exception is in the southeastern corner during the dry season. However, there are very few cirrus layers there (frequency $<$ 10% and all grid-boxes have about the same number of profiles), hence the values are more easily affected by outliers. Finally, from the histogram in Fig. 4i, the larger difference is the relative higher fraction of thin cirrus during the wet season, and higher fraction of thick cirrus during the dry season.

3.2. *Climatology: thick x thin x SVC*

We also analyzed the cirrus properties segregated according to the type of cirrus cloud: sub-visual (COD $<$0.03), thin (0.03 $<$ COD $<$ 0.3), and thick (COD $>$0.3). Results are shown in Fig. 5 and Table 2. It is important to keep in mind that CALIOP's signal becomes totally attenuated at an optical depth of about 3.55, and that the minimum detectable optical depth is about 0.002 (See tables S1 and S2 in the supplement).

There is a clear difference in base altitudes between the subvisual, thin, and thick cirrus. Subvisual cirrus layers have higher base altitudes (15 $\pm$ 1.5 km) than thin cirrus (13.6 $\pm$ 1.7 km), which are higher than thick ones (11.6 $\pm$ 1.7 km). Although all cirrus are limited in altitude by

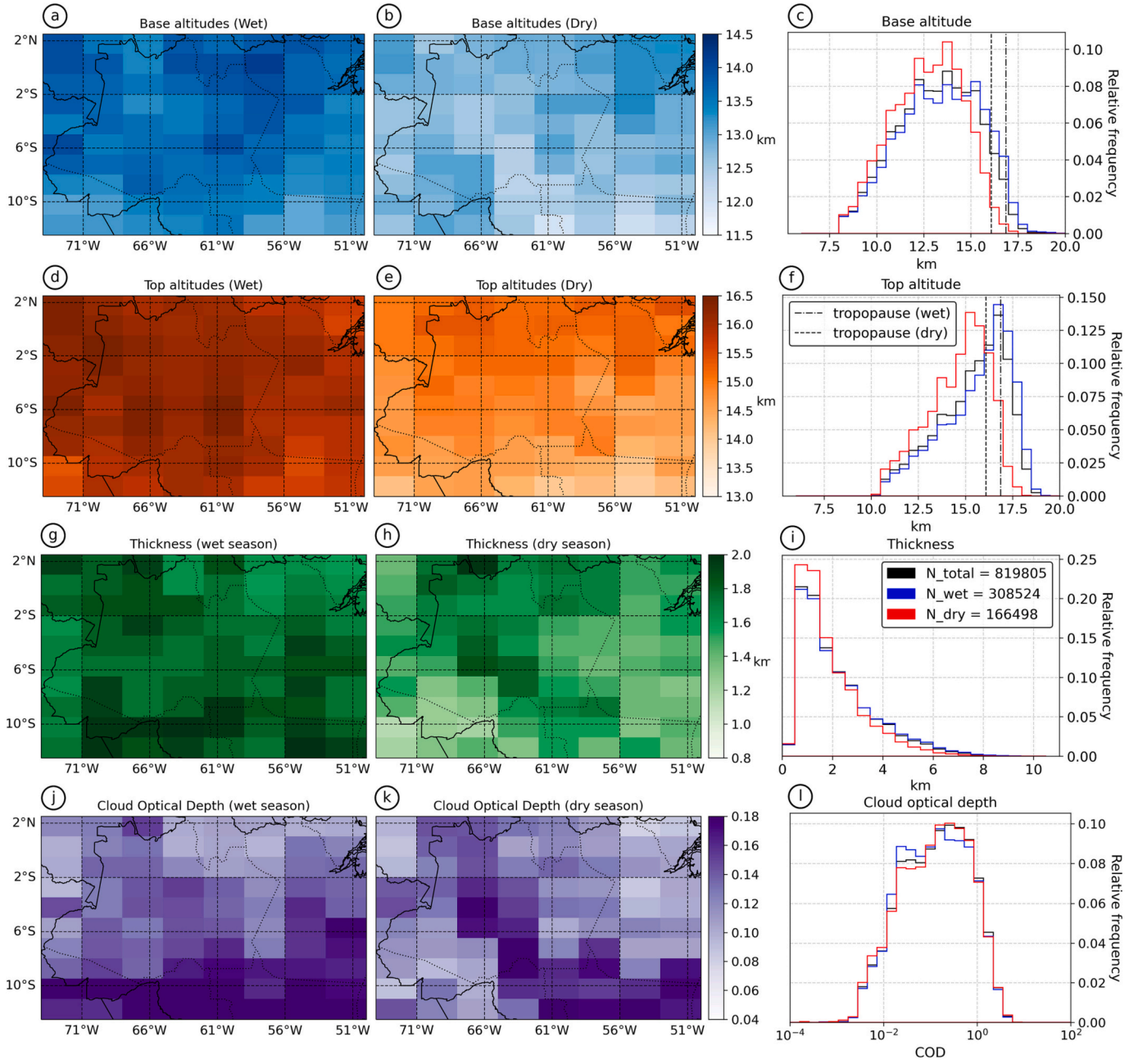

Fig. 4. Left: Maps of median base altitude (a and b), top altitude (d and e), geometric thickness (g and h) and optical depth (j and k), for the wet and dry seasons, from Jun-2009 to May-2016. Right: Normalized histograms of (c) base altitude, (f) top altitude, (i) geometric thickness, and (l) optical depth, for the wet (blue), dry (red), and full seasons (black). N_{total}, N_{wet} and N_{dry} indicate the number of total cirrus layers recorded in the full year, wet season and in the dry season, respectively. The dashed lines indicate the height of the tropopause at each season. (For interpretation of the references to colour in this figure legend, the reader is referred to the web version of this article.)

the tropopause, cloud tops are higher for subvisual (16.0 ± 1.5) and thin (15.4 ± 1.7 km) cirrus than for thick cirrus (14.8 ± 1.9 km). Moreover, there is a greater fraction of SVC cirrus at higher altitudes and exceeding the tropopause altitude. Finally, subvisual cirrus layers are considerably geometrically thinner (1.07 ± 0.56 km) than thin (1.88 ± 1.04 km) and thick (3.24 ± 1.64 km) cirrus layers, as expected given COD generally scales with the geometric thickness.

Fig. 5 also shows the spatial distribution of cirrus properties for the SVC and thick cirrus layers. There is a small spatial variability of about 5% in base and top altitudes, estimated as the difference between the maximum and minimum values in the maps. Spatial differences in geometric thickness are much greater, of about 20%. Thick layers are geometrically thicker along the northwest-southeast direction, and SVC layers are thicker in the northwest, in line with the annual mean distribution of precipitation (see Fig. S1).

These results agree with our understanding of cirrus production and dissipation, where anvils detach from convective towers, dispersing and becoming geometrically and optically thinner with time (Ackerman et al., 1988; Seifert et al., 2007; Sassen et al., 2009; Gouveia et al., 2017).

3.3. Temporal trends

Given the climatic relevance of cirrus clouds, it is important to assess whether the cirrus properties in the Amazon region show significant temporal trends. Fig. 6 shows the frequency of occurrence of cirrus in the Amazon as a function of years, and there is a clear decrease from 2009 to

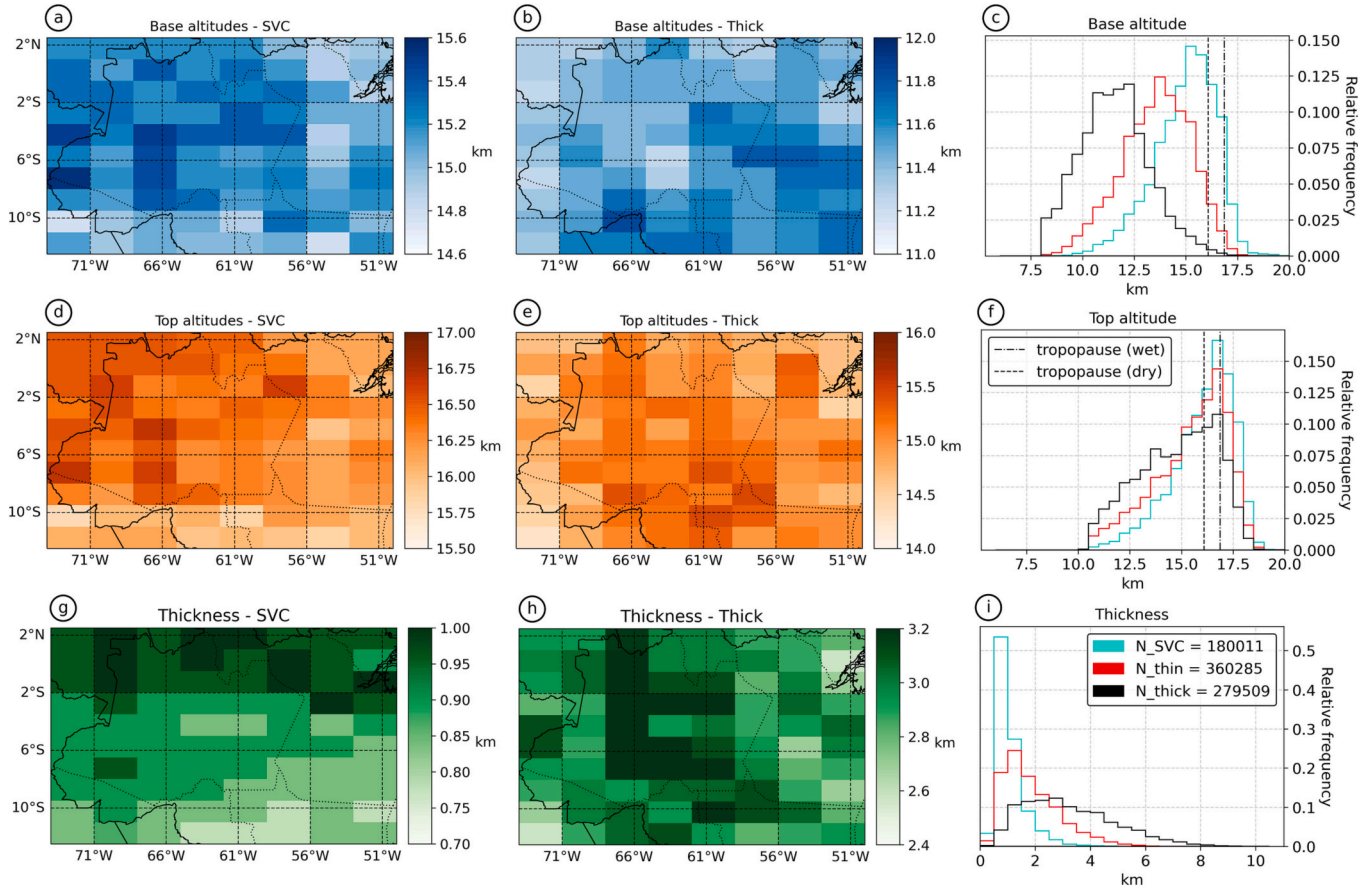

Fig. 5. Left: Maps of median base altitude (a and b), top altitude (d and e) and geometric thickness (g and h), for subvisual and thick cirrus, from 2009 to 2016. Right: Normalized histograms of (c) base altitude, (f) top altitude and (i) geometric thickness, for SVC (blue), Thin (red), and Thick clouds (black). N_{SVC}, N_{thin} and N_{thick} indicate the number of subvisual, thin and thick cirrus layers, respectively. The dashed lines indicate the height of the tropopause at wet and dry seasons. (For interpretation of the references to colour in this figure legend, the reader is referred to the web version of this article.)

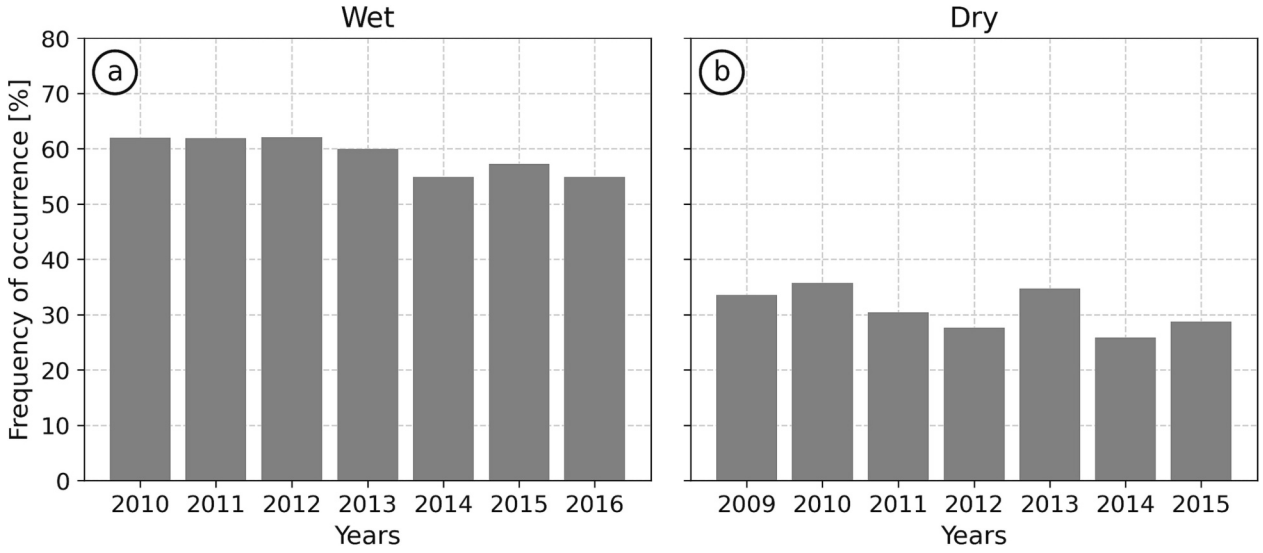

Fig. 6. Time series of the cirrus frequency of occurrence, i.e., the number of profiles with cirrus divided by the number of "good" profiles, separated into wet (a) and dry (b) seasons.

2016. In the wet season, the average rate of decrease was $1.32 \pm 0.32\%$ per year. During the dry season, despite the greater variability in the interannual scale, the rate of decrease was similar, of about $1.08 \pm 0.62\%$ per year. However, only the wet season trends is statistically significant at the 95% confidence level. These trends are larger than those of Sena et al. (2018), who found a reduction of about 0.6% per year in high cloud cover over central and eastern Amazon using geostationary satellites. With CALIOP, however, we can observe that this

change stems from a decrease in the frequency of thin and thick layers (Fig. S2).

For the cirrus properties, we analyzed the temporal trends of five percentiles: 5, 25, 50, 75, and 95-th. In the wet and dry seasons, both the base and top altitudes show no discernible trends (Fig. S3). The median base altitude increased about 1 ± 22 m per year, which is negligible and not statistically significant, while the median top altitude also didn't show a substantial trend in the wet or dry season.

This contrasts with what is observed for the time series of geometric thickness, where we can see a distinct trend for the 95-th percentile (Fig. 7a,b). However, the trends are significant only during the wet season, of about -57 ± 18 m per year. The reduction is more evident for the optically thick layers (50, 75, 95-th), but also visible for the thin (75 and 95-th) and SVC (95-th) layers (see Fig. S4). Finally, we noticed no changes for the lowest percentiles, but this is likely because CALIOP does not detect very thin layers (< 500 m).

Surprisingly, there are no changes in COD corresponding to the changes observed in geometric thickness, as can be seen in Fig. 7c,d. For all percentiles, the calculated trends are not statistically significant. We speculate this is due to the upper and lower bounds of the COD for the transparent cirrus layers, 3.55 and 0.002 respectively (Tables S1 and S2). There are cirrus with COD >3.55, but these are opaque and were hence not included in our analysis. Also, there are cirrus with COD below 0.002, but these are undetected by CALIOP's algorithm. Hence, as cirrus become optically thinner, the distribution of COD values from detected transparent cirrus still lies within the same range.

Given the large expanse of the Amazon forest, stretching north and south of the equator, temporal trends in the cirrus properties might be occurring on a smaller spatial scale than the global analysis just presented. Hence, we investigated the spatial distribution of the optical and geometric properties trends. However, we only present the maps for the variables and percentiles where a spatially consistent trend was found. Results are in Figs. 8 and 9, where the hatched areas indicate the cells with a trend classified as statistically significant.

The maps for the frequency of occurrence trends show a clear decreasing pattern over most of the Amazon. During the wet season, the frequency decreases more intensely on the edges of the area where the precipitation rate is more intense (compare with Fig. 3a). The pattern is similar during the dry season, but the frequency decreases less intensely. The geometric thickness trend maps (Fig. 9a,b) show a general reduction trend in the 95-th percentile, but mixed with localized increase trends, without a clear spatial pattern. The domain-averaged trend (Fig. 7a,b) seems to arise from specific points in the Amazon where the decrease is more expressive. The optical depth trend maps for the 5-th percentile (Fig. 9c-d) show a similar pattern, with positive and negative trends intertwined and a smaller area where the trends have significance.

Veglio and Maestri (2011) showed that geometric thickness is the main parameter that affects the shape of the backscatter and extinction profiles in semi-transparent clouds measured by CALIOP, which is closely linked with the reflectance properties of clouds, and therefore changes in cirrus geometric thickness can significantly impact their reflectance. Zhao et al. (2020) have already identified a pattern of decline in cirrus reflectance across the entire planet, which may be linked to a possible reduction in the geometric thicknesses of these clouds.

4. Conclusions

We investigated the distribution of cirrus clouds in the Amazon using 7 years of CALIOP data (Jun-2009 to Apr-2016). A total of 1,473,863 vertical profiles containing 728,123 cirrus layers were analyzed. Our climatology expanded the one presented by Gouveia (2018), with a surface lidar, and by earlier studies based on CALIOP (e.g., Massie et al., 2010; Dupont et al., 2010; Hoareau et al., 2013). The frequency of

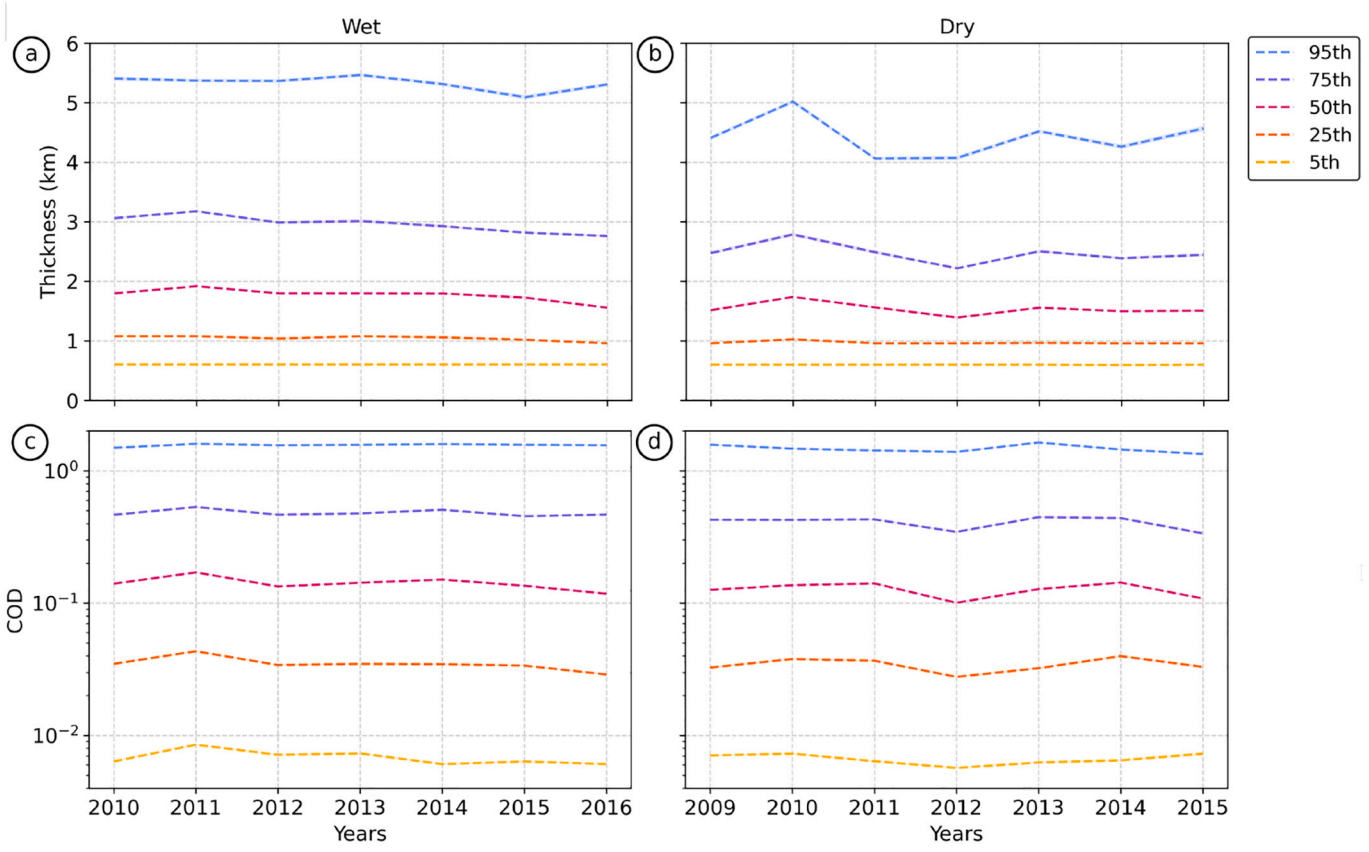

Fig. 7. Time series of the percentiles (5, 25, 50, 75, and 95-th) for geometric thickness (a-b) and COD (c-d), separated into wet and dry seasons.

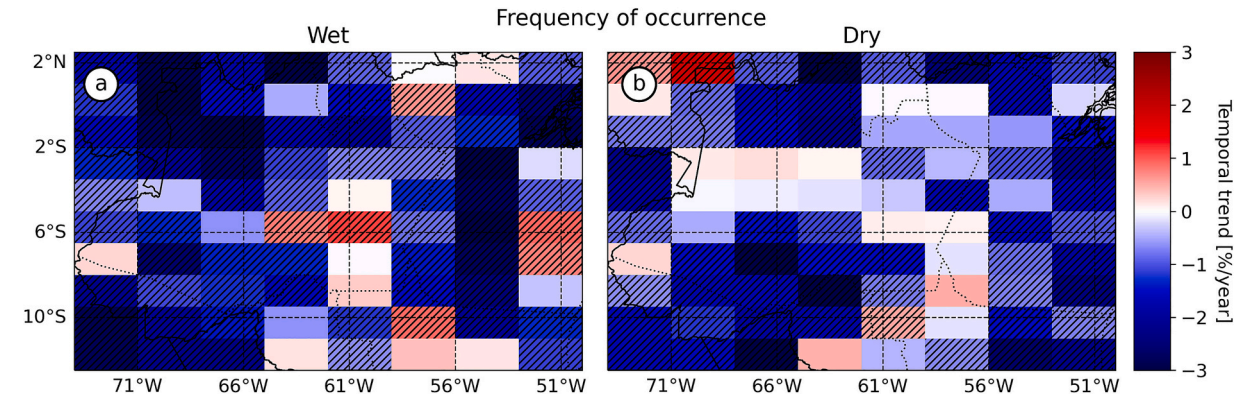

Fig. 8. Temporal trend of the frequency of occurrence, within (a) wet season and (b) dry season. The hatched areas indicate the locations where the estimated coefficient is statistically significant.

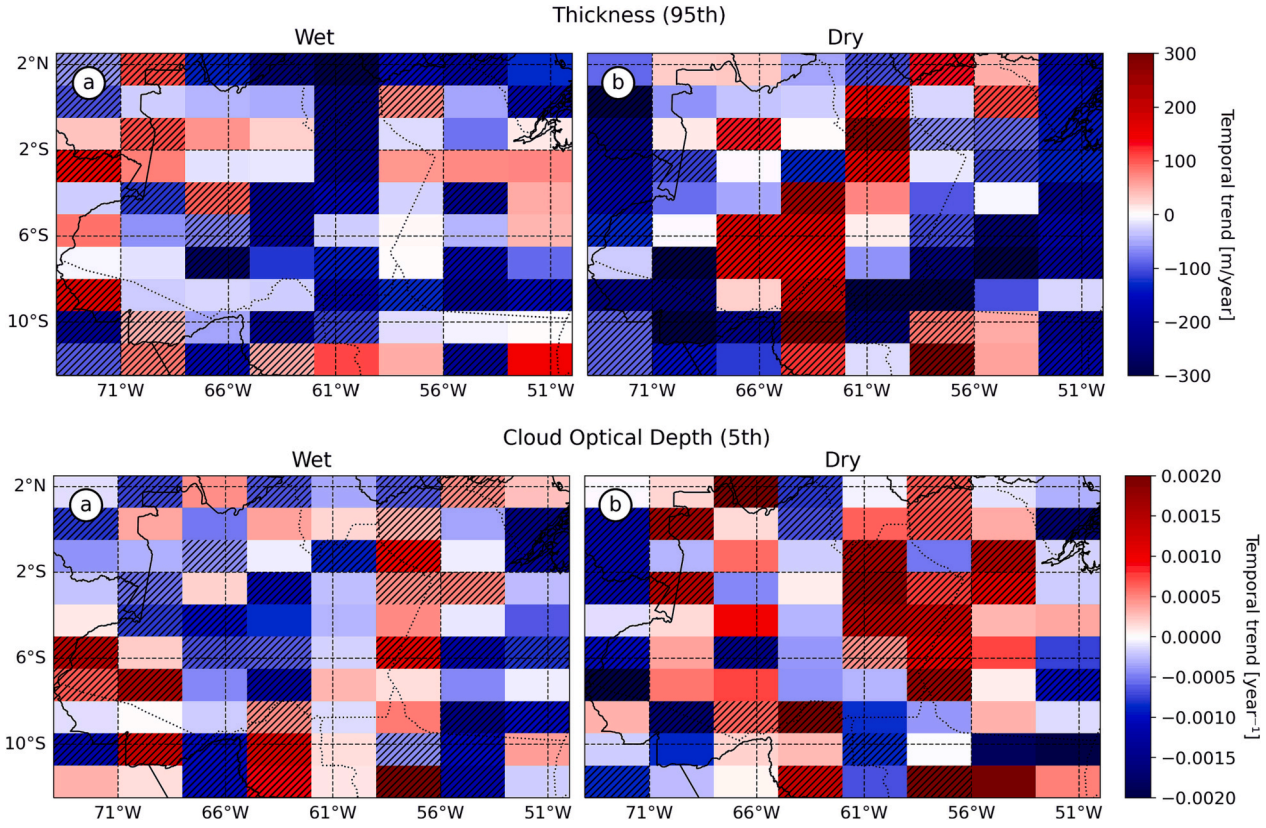

Fig. 9. Temporal trend of the 95-th percentiles of geometric thickness in the wet (a) and dry (b) seasons. The same is shown for the 5-th percentile of cloud optical depth (c and d).

occurrence showed a marked seasonal cycle, varying from 59.2% in the wet season to 31.1% in the dry season. The cloud cover was relatively uniform over the Amazon region during the wet season, and concentrated in the northwest during the dry season, in agreement with previous studies that showed that cirrus there are produced from deep convection anvils. These clouds had a base at 13.2 ± 2.1 km in altitude, a top at 15.4 ± 1.8 km, a geometric thickness of 2.16 ± 1.47 km, and an optical depth of approximately 0.38 ± 0.57. Base and top altitudes varied with the seasons because of the change in the tropopause position. The separation between the optical depth bands showed that most of the cirrus in the Amazon are optically thin (about 43.9%), while the subvisual and thick clouds correspond to 22.0 and 34.1% of the total, respectively, with no significant seasonality. Subvisual clouds were narrower (1.07 km) and mostly concentrated between 15 and 17.5 km altitude, with a higher fraction above the tropopause, while thin and thick clouds were geometrically thicker (1.88 and 3.24 km) and had a wider vertical distribution, mostly between 13 and 16 km and 10–16 km respectively.

Despite the importance of cirrus clouds to global climate, few studies used CALIOP to assess temporal trends. From our analysis, none of the percentiles (5, 25, 50, 75, and 95-th) of the distributions of cirrus base and top altitudes, for the dry and wet seasons, showed noticeable temporal trends. Similarly for the COD. However, the geometric thickness showed a consistent reduction for 50, 75, and 95-th percentiles. For the thickest percentile, the reduction was of about 60 ± 47 m per year in the dry season, and 57 ± 18 m per year during the wet season. We did not detect a trend for the lowest percentile, but this could be associated with the low sensitivity of CALIOP's algorithm to layers thinner than 500 m.

The most significant change was the reduction in the frequency of occurrence of cirrus in general over the Amazon region, one of the places where they are most abundant on the planet. There is a consistent year-round reduction of 1.3 ± 0.3% per year during the wet season and a decrease of 1.1 ± 0.6 per year during the dry season. During the wet season, this change is associated with the reduction of thin and thick cirrus, possibly due to changes in the hydrological cycle in the region. The caveat with this initial assessment is the length of the usable CALIOP data over the Amazon region.

Nonetheless, our findings corroborate the observations of Sena et al. (2018) using geostationary satellites, who found a reduction of about 0.6% per year in cloud cover over central and eastern Amazon, mainly due to changes in high clouds. However, we also observed a significant reduction in the northwest portion of the basin, where the observations used by Sena and coauthors seem to be problematic. These gradual changes in geometric thickness and frequency could lead to significant changes in cirrus reflectance and coverage in a few decades, and consequently in their impact on the radiation balance. More studies are needed to further investigate these trends, to quantify the global impact of the reduction of cirrus cover, and more importantly to investigate the reason for the reduction in convective activity over the Amazon. Finally, it is of utmost importance that future satellite missions are planned and executed in a timely manner to allow building a long-term and continuous dataset of cirrus properties that would help us better understand our changing climate.

CRediT authorship contribution statement

Ben-hur Martins Portella: Data curation, Formal analysis, Investigation, Methodology, Visualization, Writing – original draft. **Henrique de Melo Jorge Barbosa:** Conceptualization, Investigation, Supervision, Writing – review & editing.

Declaration of Competing Interest

The authors declare that they have no known competing financial interests or personal relationships that could have appeared to influence the work reported in this paper.

Data availability

The CALIOP cloud layer dataset version V4.20 used in this study can be obtained from the NASA Langley Research Center Atmospheric Science Data Center at https://asdc.larc.nasa.gov/project/CALIPSO.

Acknowledgments

We acknowledge the free use of CALIOP data sets provided by NASA. These data were obtained from the NASA Langley Research Center Atmospheric Science Data Center. This study was financed in part by Coordenação de Aperfeiçoamento de Pessoal de Nível Superior - Brasil (CAPES) - Finance Code 001.

Appendix A. Supplementary data

Supplementary data to this article can be found online at https://doi.org/10.1016/j.atmosres.2023.107167.

References

Ackerman, T.P., Liou, K.N., Valero, F.P., Pfister, L., 1988. Heating rates in tropical anvils. J. Atmos. Sci. 45, 1606–1623. https://doi.org/10.1175/1520-0469(1988)045<1606:HRITA>2.0.CO;2.

Adler, R.F., Huffman, G.J., Chang, A., Ferraro, R., Xie, P.P., Janowiak, J., Rudolf, B., Schneider, U., Curtis, S., Bolvin, D., Gruber, A., Susskind, J., Arkin, P., Nelkin, E., 2003. The Version-2 Global Precipitation Climatology Project (GPCP) Monthly Precipitation Analysis (1979–present). J. Hydrometeorol. 4, 1147–1167. https://doi.org/10.1175/1525-7541(2003)004<1147:TVGPCP>2.0.CO;2.

Arias, P., Bellouin, N., Coppola, E., Jones, R., Krinner, G., Marotzke, J., Naik, V., Palmer, M., Plattner, G.K., Rogelj, J., Rojas, M., Sillmann, J., Storelvmo, T., Thorne, P., Trewin, B., Achuta Rao, K., Adhikary, B., Allan, R., Armour, K., Bala, G., Barimalala, R., Berger, S., Canadell, J., Cassou, C., Cherchi, A., Collins, W., Collins, W., Connors, S., Corti, S., Cruz, F., Dentener, F., Dereczynski, C., Di Luca, A., Diongue Niang, A., Doblas-Reyes, F., Dosio, A., Douville, H., Engelbrecht, F., Eyring, V., Fischer, E., Forster, P., Fox-Kemper, B., Fuglestvedt, J., Fyfe, J., Gillett, N., Goldfarb, L., Gorodetskaya, I., Gutierrez, J., Hamdi, R., Hawkins, E., Hewitt, H., Hope, P., Islam, A., Jones, C., Kaufman, D., Kopp, R., Kosaka, Y., Kossin, J., Krakovska, S., Lee, J.Y., Li, J., Mauritsen, T., Maycock, T., Meinshausen, M., Min, S.K., Monteiro, P., Ngo-Duc, T., Otto, F., Pinto, I., Pirani, A., Raghavan, K., Ranasinghe, R., Ruane, A., Ruiz, L., Sallée, J.B., Samset, B., Sathyendranath, S., Seneviratne, S., Sörensson, A., Szopa, S., Takayabu, I., Tréguier, A.M., van der Hurk, B., Vautard, R., von Schuckmann, K., Zaehle, S., Zhang, X., Zickfeld, K., 2021. Technical Summary. Climate Change 2021: The Physical Science Basis. Technical Report. Cambridge University Press, Cambridge, UK and New York, USA.

Avery, M.A., Ryan, R.A., Getzewich, B.J., Vaughan, M.A., Winker, D.M., Hu, Y., Garnier, A., Pelon, J., Verhappen, C.A., 2020. CALIOP V4 cloud thermodynamic phase assignment and the impact of near-nadir viewing angles. Atmos. Measurement Techniques 13, 4539–4563. URL: https://amt.copernicus.org/articles/13/4539/2020/ https://doi.org/10.5194/amt-13-4539-2020.

Berry, E., Mace, G.G., Gettelman, A., 2019. Using A-Train Observations to Evaluate Cloud Occurrence and Radiative Effects in the Community Atmosphere Model during the Southeast Asia Summer Monsoon. J. Clim. 32, 4145–4165. https://journals.ametsoc.org/view/journals/clim/32/14/jcli-d-18-0693.1.xml. https://doi.org/10.1175/JCLI-D-18-0693.1.

Campbell, J.R., Vaughan, M.A., Oo, M., Holz, R.E., Lewis, J.R., Welton, E.J., 2015. Distinguishing cirrus cloud presence in autonomous lidar measurements. Atmos. Meas. Tech. 8, 435–449. https://doi.org/10.5194/amt-8-435-2015.

Dupont, J.C., Haeffelin, M., Morille, Y., Noël, V., Keckhut, P., Winker, D., Comstock, J., Chervet, P., Roblin, A., 2010. Macrophysical and optical properties of midlatitude cirrus clouds from four ground-based lidars and collocated CALIOP observations. J. Geophys. Res.-Atmos. 115, D00H24. https://doi.org/10.1029/2009JD011943.

Efron, B., 1982. The Jackknife, the Bootstrap and Other Resampling Plans. Society for Industrial and Applied Mathematics. URL. http://epubs.siam.org/doi/book/10.1137/1.9781611970319. https://doi.org/10.1137/1.9781611970319.

Getzewich, B.J., Vaughan, M.A., Hunt, W.H., Avery, M.A., Powell, K.A., Tackett, J.L., Winker, D.M., Kar, J., Lee, K.P., Toth, T.D., 2018. Calipso lidar calibration at 532 nm: version 4 daytime algorithm. Atmospheric. Meas. Tech. 11, 6309–6326. URL: https://amt.copernicus.org/articles/11/6309/2018/ https://doi.org/10.5194/amt-11-6309-2018.

Gouveia, D.A., 2018. Forçante radiativa, propriedades ópticas e físicas das nuvens cirrus na Amazônia. Doctoral thesis. Physics Institute, University of São Paulo. São Paulo-SP, Brazil. https://doi.org/10.11606/T.43.2019.tde-08022019-141530.

Gouveia, D.A., Barja, B., Barbosa, H.M.J., Seifert, P., Baars, H., Pauliquevis, T., Artaxo, P., 2017. Optical and geometrical properties of cirrus clouds in Amazonia derived from 1 year of ground-based lidar measurements. Atmos. Chem. Phys. 17, 3619–3636. https://doi.org/10.5194/acp-17-3619-2017.

Hoareau, C., Keckhut, P., Noel, V., Chepfer, H., Baray, J., 2013. A decadal cirrus clouds climatology from ground-based and spaceborne lidars above the south of France (43.9° N–5.7° E). Atmos. Chem. Phys. 13, 6951–6963. https://doi.org/10.5194/acp-13-6951-2013.

Hu, Y., Winker, D., Vaughan, M., Lin, B., Omar, A., Trepte, C., Flittner, D., Yang, P., Nasiri, S.L., Baum, B., Holz, R., Sun, W., Liu, Z., Wang, Z., Young, S., Stamnes, K., Huang, J., Kuehn, R., 2009. CALIPSO/CALIOP cloud phase discrimination algorithm. J. Atmos. Ocean. Technol. 26, 2293–2309. URL: http://journals.ametsoc.org/doi/10.1175/2009JTECHA1280.1 https://doi.org/10.1175/2009JTECHA1280.1.

Hunt, W.H., Winker, D.M., Vaughan, M.A., Powell, K.A., Lucker, P.L., Weimer, C., 2009. CALIPSO Lidar description and performance assessment. J. Atmos. Ocean. Technol. 26, 1214–1228. http://journals.ametsoc.org/doi/10.1175/2009JTECHA1223.1. https://doi.org/10.1175/2009JTECHA1223.1.

Kar, J., Vaughan, M.A., Lee, K.P., Tackett, J.L., Avery, M.A., Garnier, A., Getzewich, B.J., Hunt, W.H., Josset, D., Liu, Z., Lucker, P.L., Magill, B., Omar, A.H., Pelon, J., Rogers, R.R., Toth, T.D., Trepte, C.R., Vernier, J.P., Winker, D.M., Young, S.A., 2018. Calipso lidar calibration at 532 nm: version 4 nighttime algorithm. Atmos. Measurement Techniques 11, 1459–1479. URL. https://amt.copernicus.org/articles/11/1459/2018/. https://doi.org/10.5194/amt-11-1459-2018.

Larsgård, N.E., 2008. Characteristics of Cirrus Clouds over ALOMAR and their Dependence on Atmospheric Conditions. Dissertation (Ph.D.). University of Oslo, Oslo, Norway. https://www.duo.uio.no/handle/10852/12474.

Lee, J., Yang, P., Dessler, A.E., Gao, B.C., Platnick, S., 2009. Distribution and radiative forcing of tropical thin cirrus clouds. J. Atmos. Sci. 66, 3721–3731. https://doi.org/10.1175/2009JAS3183.1.

Liou, K.N., 2002. An Introduction to Atmospheric Radiation. Academic Press, Los Angeles, CA.

Liu, Z., Omar, A.H., Hu, Y., Vaughan, M.A., Winder, D.M., 2005. Part 3: Scene Classification Algorithms. CALIOP Algorithm Theoretical Basis Document. NASA Langley Research Center, Science Application International Corp., Hampton, USA. URL: https://www-calipso.larc.nasa.gov/resources/pdfs/PC-SCI-202_Part3_v1.0.pdf (Last accessed: 2023-09-15).

Lohmann, U., Lüönd, F., Mahrt, F., 2016. An Introduction to Clouds: From the Microscale to Climate. Cambridge University Press. https://doi.org/10.1017/CBO9781139087513.

Machado, L.A.T., Laurent, H., Lima, A.A., 2002. Diurnal march of the convection observed during TRMM-WETAMC/LBA. J. Geophys. Res.-Atmos. 107, 8064. https://doi.org/10.1029/2001JD000338.

Massie, S.T., Gille, J., Craig, C., Khosravi, R., Barnett, J., Read, W., Winker, D., 2010. HIRDLS and CALIPSO observations of tropical cirrus. J. Geophys. Res.-Atmos. 115, D00H11. https://doi.org/10.1029/2009JD012100.

NASA, 2018. CALIPSO Low Laser Energy Technical Advisory for Data Users. NASA Langley Research Center, Hampton, USA. URL. https://www-calipso.larc.nasa.gov/resources/calipso_users_guide/advisory/advisory_2018-06-12/CALIPSO_Laser_Energy_Technical_Advisory.pdf, 9Last accessed: 2023-08-25).

NASA, 2022. CALIPSO - Data User's Guide: Data Product Descriptions, Lidar Level 2 Cloud, Aerosol and Merged Layer v4.20 Products. URL. https://www-calipso.larc.nasa.gov/resources/calipso_users_guide/data_summaries/layer/index_v420.php.

NASA, 2023. Data Quality Summary for the CALIPSO Version 4.20 and v4.21 Lidar Level 2 Data Products. URL: https://www-calipso.larc.nasa.gov/resources/calipso_users_guide/qs/cal_lid_l2_all_v4-20.php (Last Accessed: 2023-09-19).

NASA/LARC/SD/ASDC, 2018. CALIPSO Lidar Level 2 5 km Cloud Layer, V4-20 [Data set]. Available at:. https://doi.org/10.5067/CALIOP/CALIPSO/LID_L2_05KMCLAY-STANDARD-V4-20.

Nazaryan, H., McCormick, M.P., Menzel, W.P., 2008. Global characterization of cirrus clouds using CALIPSO data. J. Geophys. Res. 113, D16211. https://doi.org/10.1029/2007JD009481.

Noel, V., Chepfer, H., Hoareau, C., Reverdy, M., Cesana, G., 2014. Effects of solar activity on noise in CALIOP profiles above the South Atlantic Anomaly. Atmospheric. Meas. Tech. 7, 1597–1603. URL. https://amt.copernicus.org/articles/7/1597/2014/. https://doi.org/10.5194/amt-7-1597-2014.

Sassen, K., Cho, B.S., 1992. Subvisual-thin cirrus lidar dataset for satellite verification and climatological research. J. Appl. Meteorol. Climatol. 31, 1275–1285. https://doi.org/10.1175/1520-0450(1992)031<1275:STCLDF>2.0.CO;2.

Sassen, K., Wang, Z., Liu, D., 2009. Cirrus clouds and deep convection in the tropics: Insights from CALIPSO and CloudSat. J. Geophys. Res. 114 https://doi.org/10.1029/2009JD011916.

Seifert, P., Ansmann, A., Müller, D., Wandinger, U., Althausen, D., Heymsfield, A.J., Massie, S.T., Schmitt, C., 2007. Cirrus optical properties observed with lidar, radiosonde and satellite over the tropical indian ocean during the aerosol-polluted northeast and clean maritime southwest monsoon. J. Geophys. Res. 112, D17205. https://doi.org/10.1029/2006JD008352.

Sena, E.T., Dias, M.A.F.S., Carvalho, L.M.V., Dias, P.L.S., 2018. Reduced wet-season length detected by satellite retrievals of cloudiness over brazilian Amazonia: a new methodology. J. Clim. 31, 9941–9964. https://doi.org/10.1175/JCLI-D-17-0702.1.

Solomon, S., Qin, D., Manning, M., Alley, R., Berntsen, T., Bindoff, N., Chen, Z., Chidthaisong, A., Gregory, J., Hegerl, G., Heimann, M., Hewitson, B., Hoskins, B., Joos, F., Jouzel, J., Kattsov, V., Lohmann, U., Matsuno, T., Molina, M., Nicholls, N., Overpeck, J., Raga, G., Ramaswamy, V., Ren, J., Rusticucci, M., Somerville, R., Stocker, T., Whetton, P., Wood, R., Wratt, D., 2007. Technical Summary. Climate Change 2007: The Physical Science Basis. Technical Report. Cambridge University Press, Cambridge, UK and New York, USA.

Stocker, T.F., Qin, D., Plattner, G.K., Tignor, M., Allen, S., Boschung, J., Nauels, A., Xia, Y., Bex, V., Midgley, P.M., 2013. Technical Summary. Climate Change 2013: The Physical Science Basis. Technical Report. Cambridge University Press, Cambridge, UK and New York, USA.

Thorsen, T.J., Fu, Q., Comstock, J.M., Sivaraman, C., Vaughan, M.A., Winker, D.M., Turner, D.D., 2013. Macrophysical properties of tropical cirrus clouds from the CALIPSO satellite and from ground-based micropulse and Raman lidars. J. Geophys. Res. Atmos. 118, 9209–9220. URL: https://agupubs.onlinelibrary.wiley.com/doi/10.1002/jgrd.50691 https://doi.org/10.1002/jgrd.50691.

Trenberth, K.E., 2022. The Changing Flow of Energy Through the Climate System. Cambridge University Press. https://doi.org/10.1017/9781108979030.

Vaillant De Guélis, T., Vaughan, M.A., Winker, D.M., Liu, Z., 2021. Two-dimensional and multi-channel feature detection algorithm for the CALIPSO lidar measurements. Atmos. Meas. Tech. 14, 1593–1613. URL. https://amt.copernicus.org/articles/14/1593/2021/. https://doi.org/10.5194/amt-14-1593-2021.

Vaughan, M.A., Winker, D.M., Powell, K.A., 2005. Part 2: Feature Detection and Layer Properties Algorithms. NASA Langley Research Center, Science Application International Corp., Hampton, USA. URL: https://www-calipso.larc.nasa.gov/resources/pdfs/PC-SCI-202_Part2_rev1x01.pdf (Last accessed: 2023-06-28).

Vaughan, M.A., Powell, K.A., Winker, D.M., Hostetler, C.A., Kuehn, R.E., Hunt, W.H., Getzewich, B.J., Young, S.A., Liu, Z., McGill, M.J., 2009. Fully automated detection of cloud and aerosol layers in the CALIPSO lidar measurements. J. Atmos. Ocean. Technol. 26, 2034–2050. URL. http://journals.ametsoc.org/doi/10.1175/2009JTECHA1228.1. https://doi.org/10.1175/2009JTECHA1228.1.

Vaughan, M.A., Winker, D.M., Powell, K.A., 2023. Data Management System - Data Products Catalog. NASA Langley Research Center, Hampton, USA. URL: https://www-calipso.larc.nasa.gov/products/CALIPSO_DPC_Rev4x95.pdf (Last accessed: 2023-06-28).

Veglio, P., Maestri, T., 2011. Statistics of vertical backscatter profiles of cirrus clouds. Atmos. Chem. Phys. 11, 12925–12943. https://doi.org/10.5194/acp-11-12925-2011.

Wilks, D.S., 2006. Statistical Methods in the Atmospheric Sciences. International Geophysics Series, Second ed. Academic Press, Amsterdam.

Winker, D.M., Pelon, J., Coakley, J.A., Ackerman, S.A., Charlson, R.J., Colarco, P.R., Flamant, P., Fu, Q., Hoff, R.M., Kittaka, C., Kubar, T.L., Treut, H.L., Mccormick, M.P., Mégie, G., Poole, L., Powell, K., Trepte, C., Vaughan, M.A., Wielicki, B.A., 2010. The CALIPSO mission: a global 3D view of aerosols and clouds. Bull. Am. Meteorol. Soc. 91, 1211–1230. https://doi.org/10.1175/2010BAMS3009.1.

Zhao, F., Tang, C., Dai, C., Wu, X., Wei, H., 2020. The global distribution of cirrus clouds reflectance based on MODIS level-3 data. Atmosphere 11. https://doi.org/10.3390/atmos11020219.

Zhu, J., 2011. Investigation on Cirrus Clouds by the Cloud-Aerosol Lidar and Infrared Pathfinder Satellite Observation Data. Dissertation (Ph.D.). University of Alaska, Fairbanks. URL: http://hdl.handle.net/11122/9096.